Evolution to aperiodic penetrative convection in odd shaped rectangular enclosures

Nadeem Hasan and Faisal M. Baig
Department of Mechanical Engineering, Aligarh Muslim University, Aligarh, India

Received January 2001
Revised April 2002
Accepted May 2002

Keywords *Numerical analysis, Navier-Stokes equations, Fluid mechanics*

Abstract *The purpose of this numerical study is to analyse the character of transition from laminar to chaotic convection in a fluid layer bounded by no-slip walls in two space dimensions for varying aspect ratio odd-shaped enclosures consisting of two rectangular chambers, with a linking horizontal enclosure. For a medium Prandtl number fluid* (Pr = 7), *the numerical solution of two-dimensional Navier-Stokes momentum and energy equations with Bousinessq approximation has been carried out. It has been found that there are finite Rayleigh numbers* Ra_1, Ra_2 *and* Ra_3 *for the onset of single, two and multiple frequency oscillatory motion at different spatial locations in the enclosure. As Ra is further increased period doubling is observed. The onset of strong chaos appears when* $Ra = Ra_3$. *This system does not revert to steady state convection at high Ra as observed by other researchers for the case of Rayleigh-Benard convection. Moreover, the period doubling transition process is consistent with the scenario of Ruelle, Takens and Newhouse. As Ra increases, the power spectrum, and time series of various dynamical variable signals, etc. all show an increasing degree of characteristics of chaos.*

Nomenclature

W	= dimensional height and width of the enclosure, m
L	= width of the vertical and horizontal legs of the enclosure, m
AR_L	= leg aspect ratio L/W
g	= acceleration due to gravity, m/s^2
ν	= kinematic viscosity of fluid, m^2/s
κ	= thermal diffusivity, m^2/s
β	= coefficient of thermal expansion $-(1/\rho)(\partial\rho/\partial T)$, 1/K
T_c	= temperature of cold wall, K
T_h	= temperature of hot wall, K
δT	= temperature difference between hot and cold walls, $T_h - T_c$, K
Pr	= Prandtl number of fluid ν/κ
Ra	= Rayleigh number $g\beta W^3\delta T/(\nu\kappa)$
U	= dimensional vector velocity of fluid particle, m/s
V = (u, v)	= dimensionless vector velocity of fluid particle $(U\,W)/\kappa$
p	= dimensional pressure of fluid in motion, N/m^2
T	= dimensional temperature of fluid particle in motion
p_h	= dimensional pressure of fluid at rest, N/m^2
ρ_o	= density of fluid at rest, Kg/m^3
P	= non-dimensional pressure $(p - p_h)W^2/\rho_o\kappa^2$
θ	= non-dimensional temperature $(T - T_c)/\delta T$
ψ	= non-dimensional stream function
$\forall$	= non-dimensional dilatation rate of fluid particle $\nabla\cdot\mathbf{V}$
Ke	= non-dimensional kinetic energy per unit mass of the fluid particle, $\frac{1}{2}(u^2 + v^2)$
Δ	= Laplacian operator ∇^2
δt	= non-dimensional time step

International Journal of Numerical Methods for Heat & Fluid Flow, Vol. 12 No. 8, 2002, pp. 895-915.

DOI 10.1108/09615530210448697

Introduction

The problem of fluid flow driven by buoyancy forces is an excellent candidate for attempting to understand the bifurcations and the changes in the flow patterns as some control parameter is varied. This is because such flows represent one of the simplest coupled non-linear problems of fluid flows. The problem of natural convection in enclosures has received much attention for the past 30 years because of their importance in such diverse areas as meteorology, geophysics, astrophysics, nuclear reactor systems, materials processing, solar energy systems, thermal energy storage systems and chemical, food and metallurgical industries. An excellent survey is performed by Ostrach (1988) on natural convection in enclosures. So far, both experimental and numerical studies have revealed that as the main control parameter known as the Rayleigh number (Ra), which is a relative measure of destabilizing forces of buoyancy to the stabilizing forces of viscosity and thermal diffusivity, is increased the flow undergoes a series of transitions from steady to periodic to quasi periodic leading to a chaotic motion. Most of the studies carried out by Baig and Asrar (1995), Curry *et al.* (1984), Mohamad and Viskanta (1990), Yang (1988), Yang and Mukutmoni (1993a, b) for studying the development of chaotic convection, have been performed on regular rectangular enclosures.

More recently, researchers have started focussing attention on odd geometries and few studies with irregular geometries have been reported in the literature. Natural convection within enclosures of general irregular geometry with differentially heated walls was dealt by Coulter and Guceri (1987). Glakpe and Asfaw (1991) studied natural convection in enclosures with inner bodies of arbitrary shapes. Nithiarasu *et al.* (1995) have studied natural convection in inverted L-shaped enclosures. Raji *et al.* (1997) studied natural convection in cavities interacting with each other through fluid motion.

The present work deals with study of transition from laminar to quasi-periodic natural convection followed by chaotic advection in an odd-shaped enclosure comprising of two rectangular enclosures linked by a cold wall at the top and a hot wall at the bottom (Figure 1). The present configuration represents a basic configuration for the study of room ventilation, involving the association of two chambers or cells which communicate laterally through an opening, in the same manner as two rooms connected through a doorway, window, or over an incomplete dividing wall. Some experimental and computational studies have been carried out in similar configurations providing flow pattern and heat transfer data for both air and water filled enclosures. Blay *et al.* (1998) studied heat transfer through a horizontal aperture connecting two non-isothermal rooms. Otis and Jones (1987), studied natural convection in partially divided enclosures. Since the present study involves a fluid with $Pr = 7.0$, the results may not be directly useful for problems involving room ventilation, however, the present study does provide some insight into the various trends regarding the flow pattern and transitions from steady to unsteady motions.

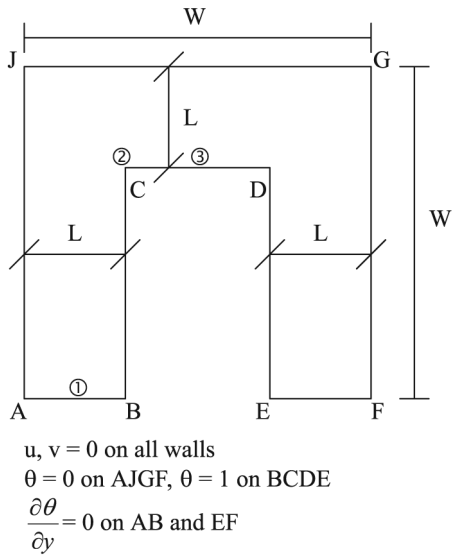

Figure 1.
Odd shaped enclosure showing locations of spatial points ①, ② and ③

Another possible application of the present problem is in the design of liquid cooled heat sinks. Liquid cooled heat sinks provide the highest thermal performance per unit volume and, when optimally designed, can exhibit a very low thermal resistance. The space between the vertical legs of the enclosure (Figure 1) can be utilised to mount the enclosure as a heat sink over some heat dissipating object or device. Liquid cooled heat sinks are employed in some thermoelectric or Peltier heat pumps.

To the best of the knowledge of the authors, none of the researchers have studied the problem in the present geometry of the enclosure, with the chosen boundary conditions, from the viewpoint of chaotic advection. Among the possible routes to chaotic convection, Ruelle *et al.* (1978) suggest a scenario in which by varying a control parameter like Ra a stationary solution changes to a limit cycle. The periodic limit cycle changes into a quasi-periodic T^2 torus having two incommensurate frequencies. Further increase in the control parameter changes the T^2 torus to a T^3 torus or to a chaotic solution. The other routes to chaos are subharmonic cascading as suggested by Fiegenbaum (1978) or through generation of intermittent chaos. We have studied the routes of transition to chaos in an odd-shaped two-dimensional rectangular enclosure and also observed the change in spatio-temporal dynamics brought by the modified geometry by varying the leg aspect ratios AR_L.

According to Curry *et al.* (1984) there might be four Ra that distinguish various flow regimes at different spatial locations, namely: Ra_c, critical Ra at which convection rolls appear; Ra_1, Ra at which rolls undergo a bifurcation to a periodic oscillatory state; Ra_2, Ra number at which two frequency oscillatory

flow develops; Ra_3, Ra above which three frequency or higher quasi-periodic flow develops and might be coincident with chaotic motion.

Our objective specifically are twofold namely, to check for the existence of any one of these four Ra in a no-slip, two-dimensional odd-shaped rectangular enclosure for medium Prandtl number fluid, and to ascertain the basic trends in spatial and temporal patterns of flow with increase of Ra and AR_L.

Formulation and numerical technique

The dimensionless governing equations of continuity, momentum, and energy in two-dimension with Boussinesq approximation are given by:

$$\frac{\partial u}{\partial x} + \frac{\partial v}{\partial y} = 0 \tag{1}$$

$$\frac{\partial u}{\partial t} = H - \frac{\partial p}{\partial x} \tag{2}$$

$$\frac{\partial v}{\partial t} = G - \frac{\partial p}{\partial y} \tag{3}$$

$$\frac{\partial \theta}{\partial t} = F \tag{4}$$

where

$$H = -u\frac{\partial u}{\partial x} - v\frac{\partial u}{\partial y} + \mathrm{Pr}\Delta u \tag{5}$$

$$G = -u\frac{\partial v}{\partial x} - v\frac{\partial v}{\partial y} + \mathrm{Ra}\,\mathrm{Pr}\,\theta + \mathrm{Pr}\Delta v \tag{6}$$

$$F = -u\frac{\partial \theta}{\partial x} - v\frac{\partial \theta}{\partial y} + \Delta\theta \tag{7}$$

The reference length, velocity and time used are W, κ/W and W^2/κ, respectively. The Prandtl number of the fluid is taken as 7. No-slip boundary conditions are employed for u and v on all the walls. The boundary conditions together with the geometry of the flow domain can be seen in Figure 1.

In the present work, the finite difference method is used to solve the coupled elliptic equations on a structured, non-staggered grid. The grids employed for different AR_L are shown in Figure 2. At lower Ra ($<10^7$) 51×51 mesh is employed while at higher Ra i.e. at $\mathrm{Ra} = 10^7$, a 81×81 grid is employed.

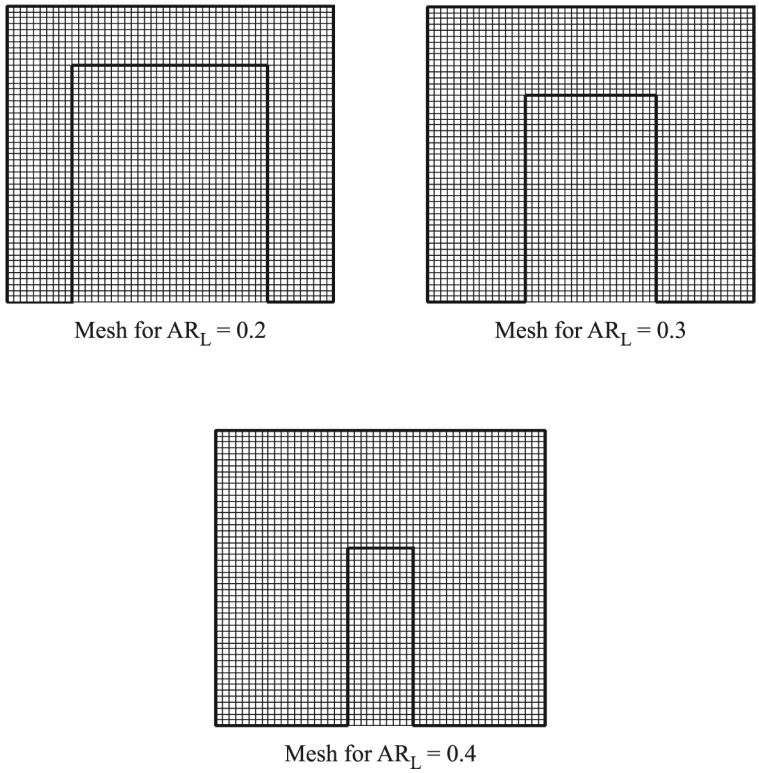

Figure 2.
Grids employed for different leg aspect ratios AR_L

The non-linear terms in equations (2)-(4) have been evaluated by a variant of quadratic upstream interpolation for convection kinematics QUICK scheme as proposed by Leonard (1979). The diffusion terms are discretized using the three point central differencing stencil, while the time integration has been performed explicitly using Euler's scheme in order to capture the unsteady physics especially of the oscillatory flow regime.

Thus the non-dimensional velocity components and temperature at new time level $n + 1$ and at each grid point (i, j) are obtained from equations (2)-(4) as follows:

$$u_{i,j}^{n+1} = u_{i,j}^{n} + \left\{ H_{i,j}^{n} - \left(\frac{\partial p}{\partial x} \right)_{i,j}^{n} \right\} \delta t \tag{8}$$

$$v_{i,j}^{n+1} = v_{i,j}^{n} + \left\{ G_{i,j}^{n} - \left(\frac{\partial p}{\partial y} \right)_{i,j}^{n} \right\} \delta t \tag{9}$$

$$\theta_{i,j}^{n+1} = \theta_{i,j}^{n} + \{F_{i,j}^{n}\}\,\delta t \tag{10}$$

The velocity field computed from equations (8) and (9) must be divergence free. This is enforced through pressure by forcing the pressure to satisfy a Poisson equation at time level n, obtained by taking divergence of the discrete momentum equation i.e. by applying the discrete operator $\delta/\delta x$ to equation (8) and $\delta/\delta y$ to equation (9). This results in the following discrete Poisson equation:

$$\begin{aligned}\frac{\delta}{\delta x}\left(\frac{\partial p}{\partial x}\right)_{i,j}^{n} + \frac{\delta}{\delta y}\left(\frac{\partial p}{\partial y}\right)_{i,j}^{n} = {} & \frac{\delta}{\delta x}(H)_{i,j}^{n} + \frac{\delta}{\delta y}(G)_{i,j}^{n} + \left(\frac{1.0}{\delta t}\right) \\ & \times \left[\frac{\delta}{\delta x}(u)_{i,j}^{n} + \frac{\delta}{\delta y}(v)_{i,j}^{n}\right] - \left(\frac{1.0}{\delta t}\right) \\ & \times \left[\frac{\delta}{\delta x}(u)_{i,j}^{n+1} + \frac{\delta}{\delta y}(v)_{i,j}^{n+1}\right]\end{aligned} \tag{11}$$

Since it is desired that the velocity components satisfy the continuity condition at the new time level $n + 1$, the last term on the right hand side of equation (11) is forced to be zero. The pressure field obtained from the discrete Poisson equation (11) therefore is employed in equations (8) and (9) to obtain velocities at the new time level. This procedure is discussed in detail by Ferziger and Peric (1996).

The pressure Poisson equation requires some care in the discretization on a non-staggered grid as improper discretization may lead to spurious grid scale pressure oscillations. The discretisation of the various terms in the pressure Poisson equation is done as follows:

$$\frac{\delta}{\delta x}\left(\frac{\partial p}{\partial x}\right)_{i,j}^{n+1} \cong \frac{\left[\left(\frac{\partial p}{\partial x}\right)_{i+\frac{1}{2},j}^{n} - \left(\frac{\partial p}{\partial x}\right)_{i-\frac{1}{2},j}^{n}\right]}{[(\mathrm{d}x)_1 + (\mathrm{d}x)_2]/2} \tag{12}$$

$$\left(\frac{\partial p}{\partial x}\right)_{i+\frac{1}{2},j}^{n} \cong \frac{(p_{i+1,j}^{n} - p_{i,j}^{n})}{(\mathrm{d}x)_1} \tag{13}$$

$$\left(\frac{\partial p}{\partial x}\right)_{i-\frac{1}{2},j}^{n} \cong \frac{(p_{i,j}^{n} - p_{i-1,j}^{n})}{(\mathrm{d}x)_2} \tag{14}$$

$$\frac{\delta}{\delta x}(H)^n_{i,j} \cong \frac{\left[(H)^n_{i+\frac{1}{2},j} - (H)^n_{i-\frac{1}{2},j}\right]}{[(\mathrm{d}x)_1 + (\mathrm{d}x)_2]/2} \tag{15}$$

$$\frac{\delta}{\delta x}(u)^n_{i,j} \cong \frac{\left[(u)^n_{i+\frac{1}{2},j} - (u)^n_{i-\frac{1}{2},j}\right]}{[(\mathrm{d}x)_1 + (\mathrm{d}x)_2]/2} \tag{16}$$

The values of $H_{i+\frac{1}{2},j}$ and $H_{i-\frac{1}{2},j}$ are obtained by linear interpolation using the adjacent nodes.

However, the values of $u_{i+\frac{1}{2},j}$ and $u_{i-\frac{1}{2},j}$ are not obtained through linear interpolation from adjacent nodes as this would lead to spurious pressure oscillations. These velocities are obtained as follows:

$$u^n_{i+\frac{1}{2},j} = 0.5(u^n_{p_{i,j}} + u^n_{p_{i+1,j}}) - \delta t \frac{(p^n_{i+1,j} - p^n_{i,j})}{(\mathrm{d}x)_1} \tag{17}$$

The grid spacings in equations (12)-(17) are defined as follows:

$$(\mathrm{d}x)_1 = x_{i+1} - x_i \tag{18a}$$

$$(\mathrm{d}x)_2 = x_i - x_{i-1} \tag{18b}$$

The velocity u_p in equation (17) is obtained from the momentum equation without the pressure gradient term as follows:

$$u^{n+1}_{p_{i,j}} = u^n_{i,j} + \left\{H^n_{i,j}\right\} \delta t \tag{19}$$

This procedure closely resembles the momentum interpolation employed in the finite volume method and is discussed in detail by Ferziger and Peric (1996).

The Poission equation (11) has been solved subject to Neumann boundary conditions for pressure obtained by applying momentum equations at the wall. The SIP procedure (ILU decomposition) has been employed for the Poisson equation with a tolerance of 1.0×10^{-9}. A dimensionless time step of 1×10^{-4} for $\mathrm{Ra} \leq 10^4$, 1×10^{-5} for $\mathrm{Ra} \in [10^4, 10^5]$, 1×10^{-6} for $\mathrm{Ra} \in [10^5, 10^6]$ and 1×10^{-7} for $\mathrm{Ra} \in [10^6, 10^7]$ has been used to advance the time integration in order to keep the dilation $\forall$ always less than 0.001.

In order to check for grid independence the simulations were carried out on a 41×41 and 51×51 uniform mesh. The results for these two grids differed by less than 1 per cent, thus indicating the grid independence of the results.

Validation studies

The numerical code developed has been validated by solving the glazing problem i.e. buoyancy driven flow inside a square cavity with two differentially

heated vertical walls and two adiabatic horizontal walls. The results have been compared with the benchmark solutions of Nonino and Croce (1997) and de Vahl Davis (1983). The range of Ra considered is between 10^5 and 10^7 while Pr is taken to be 0.71. Table I shows the comparison between the results of present study and benchmark solution. The maximum and minimum grid spacing employed was 0.04 and 0.004, respectively, with total number of grid points being equal to 55, in both space directions as in the benchmark study. Deviation of results from the benchmark solution is observed to be less than 1 per cent for the various parameters. The solutions of de Vahl Davis are upto $Ra = 10^6$ only. The pressure fields obtained were smooth and free from any spurious oscillations.

Results and discussion

Natural convection in the odd shaped enclosure (Figure 1) is studied by observing spatial and temporal patterns of flow. The Ra is varied from 10^5 to 10^7 for three $AR_L = 0.2$, 0.3 and 0.4. The following sections discuss the trends that were found in the spatial and temporal dynamics of flow in the odd shaped enclosure.

Spatial dynamics: general trends

As Ra is increased from 10^5 to 10^7, the flow pattern in space undergoes a change, from a spatially symmetric flow pattern with convection concentrated more in vertical legs (Ra 10^5-10^6) to an unsymmetric multicellular and to an unsymmetric penetrative convection (Ra 10^6-10^7) with convection dominating in horizontal leg. This can be readily discerned from the contour plots of isotherms and streamlines shown in Figure 3(a)-(d) for $AR_L = 0.3$. The isotherms are plotted in the range [0,1] and the ranges of the stream functions are given in the figure captions. The flow patterns depicted for $10^5 \leq Ra \leq 10^6$ are steady flow fields whereas those for $10^6 \leq Ra \leq 10^7$ are instantaneous snapshots of unsteady flow fields. This trend indicates that the fluid confined

Table I. Validation of code with numerical results of Nonino and de Vahl Davis

Ra	$\lvert\psi\rvert_{max}$	U_{max}	V_{max}	Nu_{avg}	Nu_{max}	Nu_{min}	Reference
10^5	9.67	35.21	69.10	4.52	7.68	0.74	Present
10^5	9.61	34.73	68.59	4.51	7.72	0.73	de Vahl Davis
10^5	9.62	34.75	68.65	4.52	7.73	0.72	Nonino
10^6	16.89	66.11	222.77	8.82	17.49	1.00	Present
10^6	16.75	64.63	219.36	8.82	17.92	0.99	de Vahl Davis
10^6	16.82	64.83	220.63	8.82	17.56	0.98	Nonino
10^7	31.40	152.23	708.54	16.25	38.98	1.38	Present
10^7	30.16	148.60	699.67	16.52	39.47	1.38	Nonino

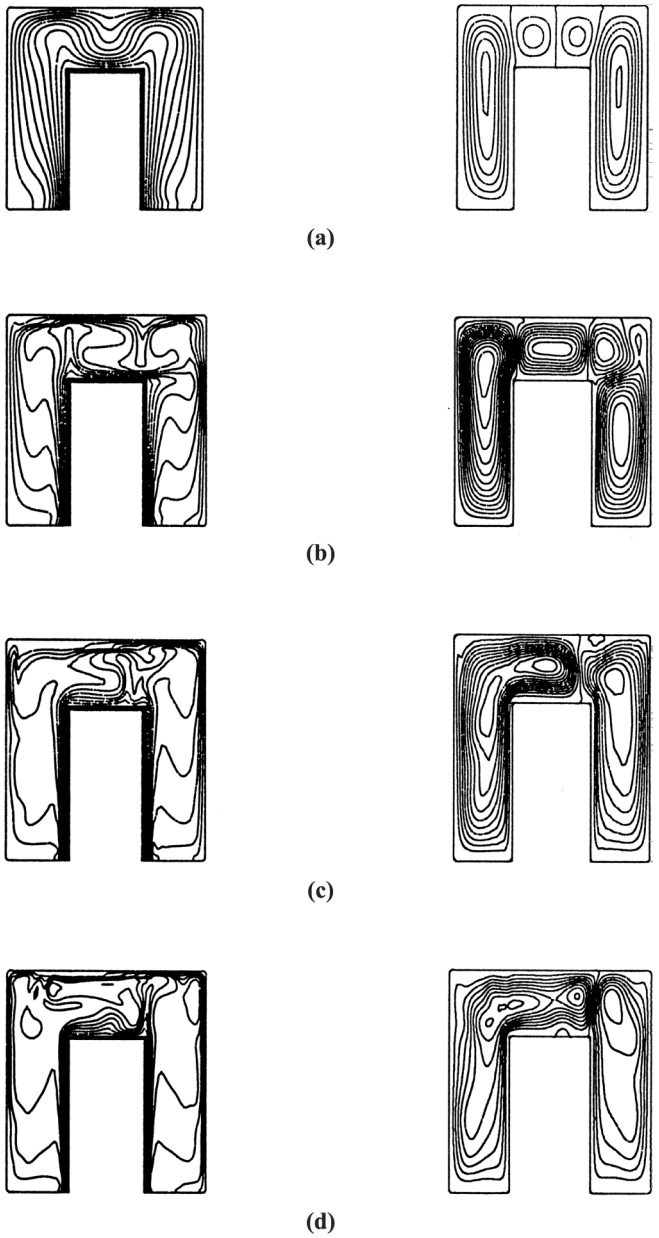

Figure 3.
Contour plots of isotherms and streamlines for $AR_L = 0.3$ and at (a) $Ra = 10^5$, $\Psi \in [-5.5, 5.1]$; (b) $Ra = 10^6$, $\Psi \in [-27.9, 19.9]$; (c) $Ra = 4 \times 10^6$, $\Psi \in [-59.0, 43.5]$; (d) $Ra = 10^7$, $\Psi \in [-62.1, 69.2]$

in the vertical legs is less stable to stratification than the fluid confined in the horizontal leg. This is particularly evident as one observes the total absence of convection in the horizontal leg for $Ra = 10^5$, $AR_L = 0.2$ as shown in Figure 4. While the differential heating of the side walls of the vertical legs inevitably

causes circulation loops or rolls, the convection in the horizontal leg is the outcome of two distinct phenomenons:

(1) generation of convective loop by buoyant elements generated from the bottom heated wall of the horizontal leg;

(2) buoyant elements of fluids penetrating the horizontal leg from the vertical legs.

Figures 5 and 6 clearly indicate that the convection rolls generation in the horizontal leg is encouraged by an increase in the Ra while simultaneously it is discouraged by a decrease in the AR_L. This is so because a decrease in the AR_L essentially amounts to a decrease in the thickness of fluid layer in the horizontal leg leading to enhanced stability of the layer. Figures 5 and 6 also indicate that, the ability of penetration of buoyant elements into the horizontal leg is increased by increasing the Ra (the buoyant elements being more energetic), while the penetrative effect is mitigated by lowering the AR_L. This is so because a decrease in AR_L decreases the kinetic energy Ke of the convecting buoyant elements in the vertical legs as shown in Figure 7(a)-(c).

Therefore the overall spatial dynamics essentially can be split into two regimes:

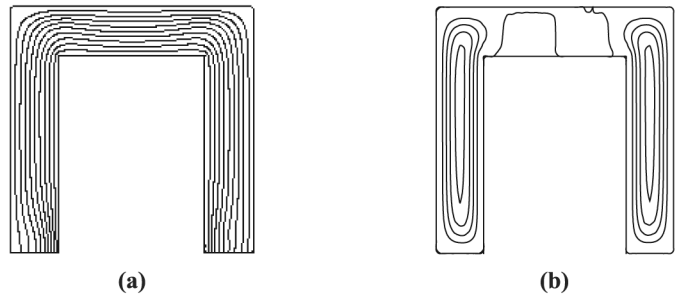

Figure 4.
Contour plots of isotherms and streamlines for $AR_L = 0.2$ and at $Ra = 10^5$, $\Psi \in [-2.2, 2.2]$

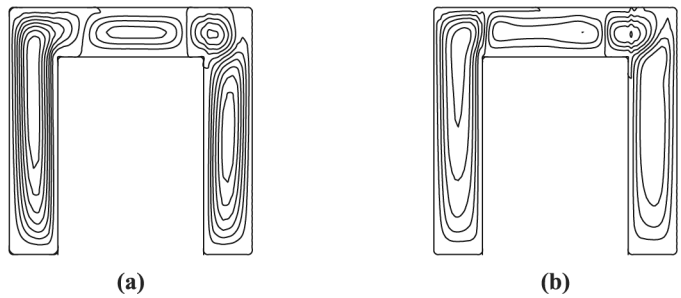

Figure 5.
Contour plots of streamlines at $AR_L = 0.2$ and at (a) $Ra = 10^6$, $\Psi \in [-15.8, 13.5]$; (b) $Ra = 10^7$, $\Psi \in [-56.7, 39.0]$

(1) spatial dynamics in the vertical legs which is somewhat insensitive to changes in AR_L and Ra in the range considered;

(2) spatial dynamics in the horizontal legs which is sensitive to changes in AR_L and Ra.

Thus the spatial dynamics at any given AR_L and Ra reflects the outcome of the competition between the penetration phenomena and convective motion generation in the horizontal leg. At lower AR_L (0.2) the phenomenon of non-penetrative convection in horizontal leg dominates for $10^5 \leq Ra \leq 10^7$ because Ke of elements in vertical legs is not sufficient enough for penetrative motion to occur. This means that there is a threshold Ke of buoyant elements in vertical legs for penetrative motion to occur. For medium AR_L (0.3) the convection generation in horizontal leg dominates for $10^5 \leq Ra \leq 10^6$ while penetration phenomenon dominates for $10^6 \leq Ra \leq 10^7$. At high AR_L (0.4) the penetration phenomenon dominates for $10^5 \leq Ra \leq 10^7$. Finally, it can be inferred that penetrative convection is favoured at higher AR_L (0.3-0.4) and Ra (10^6-10^7) while non-penetrative convection in the horizontal leg is favoured at lower AR_L (0.2-0.3) and Ra (10^5-10^6).

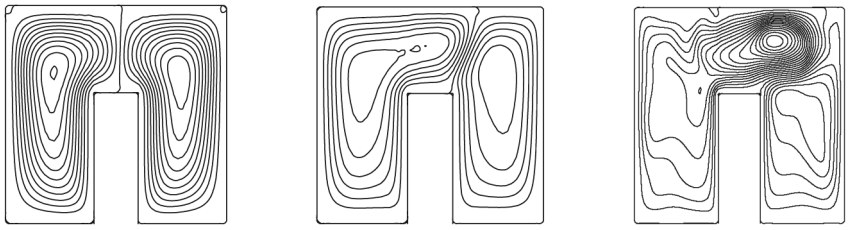

Figure 6.
Contour plots of streamlines at $AR_L = 0.4$ and at (a) $Ra = 10^5$, $\Psi \in [-11.1, 10.8]$; (b) $Ra = 10^6$, $\Psi \in [-33.5, 20.0]$; (c) $Ra = 10^7$, $\Psi \in [-168.0, 57.3]$

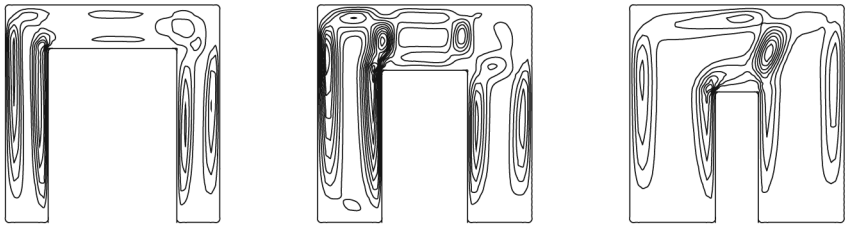

Figure 7.
Iso-kinetic energy contours at $Ra = 10^6$ for (a) $AR_L = 0.2$, $K \in [0.0, 29560]$; (b) $AR_L = 0.3$, $K \in [0.0, 52620]$; (c) $AR_L = 0.4$, $K \in [0.0, 80033]$

Temporal dynamics: general trends

To study the temporal dynamics the time history of all the dynamical variables was recorded at three different spatial points marked as ①, ② and ③ as shown in Figure 1. The non- dimensional coordinates of these points are $(0.5 \times AR_L,\ 0.02)$, $(AR_L - 0.02,\ 1.0 - AR_L + 0.02)$ and $(0.5,\ 1.0 - AR_L + 0.02)$, respectively. Spectral analysis is used to identify patterns in the temporal behaviour through identification of dominant frequencies. For this purpose, the discrete time series of u is transformed into frequency domain by applying a Fast Fourier Transform (FFT) from which the power spectrum $P(u)$ is obtained by determining the square of the magnitude of each term in the discrete FFT. The power spectrum is plotted against the ratio of the non-dimensional frequency f to the non-dimensional sampling frequency f_{max} of the discrete time series.

It was found that for $10^5 \leq \mathrm{Ra} < 10^6$ and for $0.2 \leq AR_L \leq 0.4$ the flow always attained a steady state. Figure 8(a)-(c) shows the changes that take place in the temporal behaviour for $AR_L = 0.3$ with increase in Ra at point ①. The flow undergoes the first transition from steady to periodic at $\mathrm{Ra} = 10^6$. In Figure 8(a) the time history of local rate of change of temperature is depicted instead of the time history of velocity u. This is because the periodic nature of the flow is more clearly brought about in this plot than in the time history of velocity u. At $\mathrm{Ra} = 4 \times 10^6$, the flow is quasi-periodic with three dominant frequencies as can be seen from the power spectrum in Figure 8(b). Finally, one observes the chaotic convection with a broad based power spectrum (see Figure 8(c)). These temporal patterns are observed at all the three locations. With increase in Ra the following can be observed:

(1) the fluctuations become more and more energetic (increase in power in various frequencies);

(2) broadening of the frequency spectrum with higher and higher frequencies being excited culminating into a chaotic state;

(3) a shift in the concentration of energy in the lower frequencies towards the higher ones.

The last observation can be made on the basis of a shift in the most dominant frequency from lower end to the higher end of the spectrum. This general trend in the temporal dynamics is observed at all the AR_L.

The effect of AR_L on the temporal dynamics can be seen from Figure 9(a)-(c) where the time history and power spectrum of horizontal velocity component u at point (1) are shown. It is evident that a decrease in the AR_L suppresses the frequency content of the spectrum. Not only the number of active frequencies are suppressed but the intensity of fluctuations is also reduced. Thus it can be concluded that reduction in AR_L has a stabilizing effect.

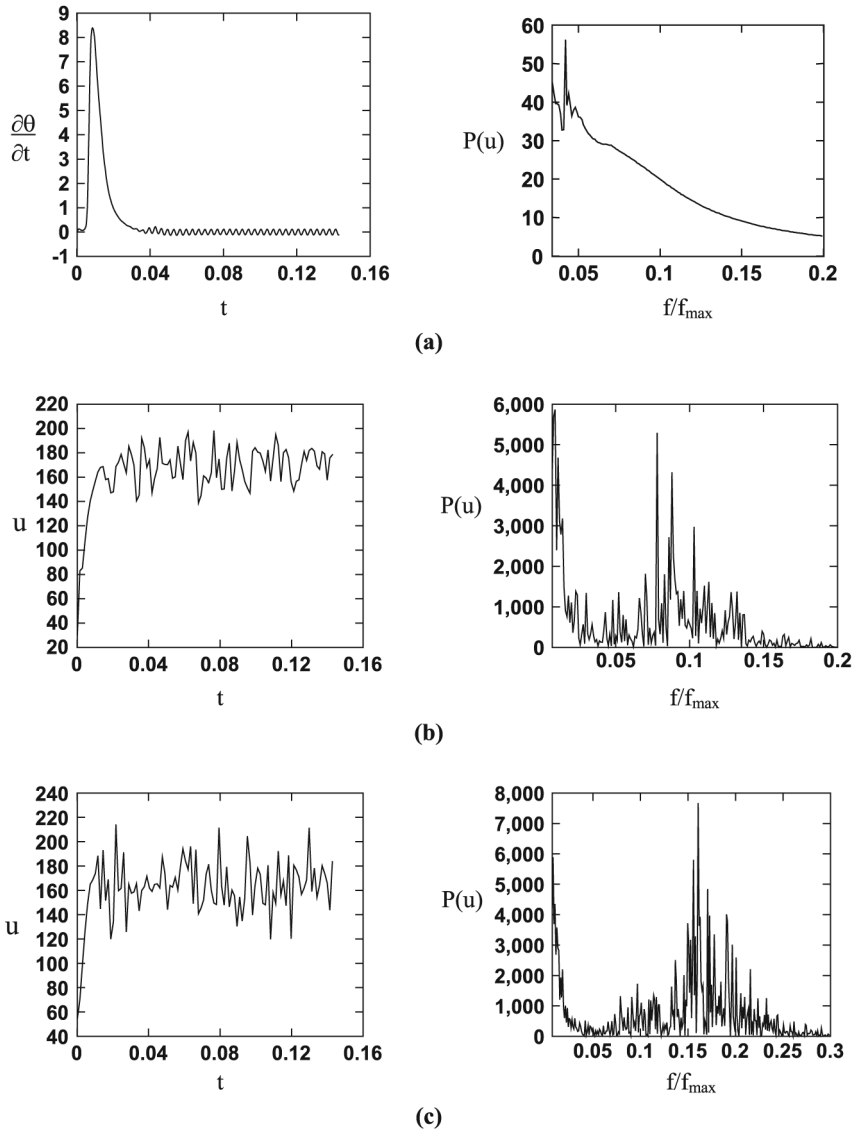

Figure 8.
Time history and power spectrum plots for $AR_L = 0.3$ at point ① at (a) Ra $= 10^6$; (b) Ra $= 4 \times 10^6$; (c) Ra $= 10^7$

Connection between the spatial and the temporal dynamics

A connection between the spatial and the temporal dynamics can be established if one observes the temporal behaviour at the three spatial points at the same AR_L and Ra. Figure 10(a)-(c)shows the time history plots of u at the three spatial points for $AR_L = 0.2$ and Ra $= 4 \times 10^6$. It can be observed that while the flow is nearly periodic at all the three points the frequency of

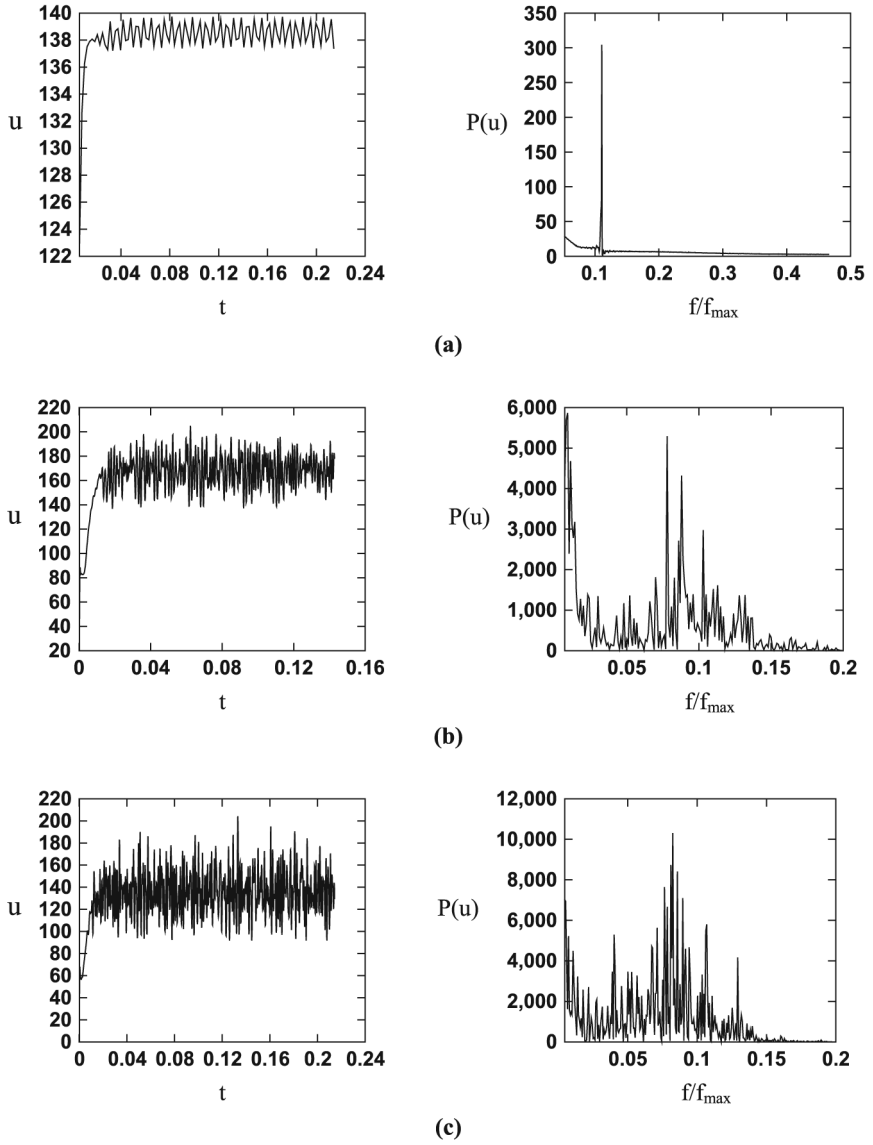

Figure 9.
Time history and power spectrum plots of velocity u at Ra $= 4 \times 10^6$ at point ① at (a) $AR_L = 0.2$; (b) $AR_L = 0.3$; (c) $AR_L = 0.4$

oscillation is higher at point ① than at point ③ with the lowest frequency at point ②. This supports the earlier proposed spatial dynamics that at lower AR_L (0.2) the penetrative convection is not able to dominate in the horizontal leg and therefore the fluctuations in the horizontal and the vertical legs are solely due to their own buoyancy generated convective currents. Higher frequency fluctuations in the vertical leg is an indication of the fact that for

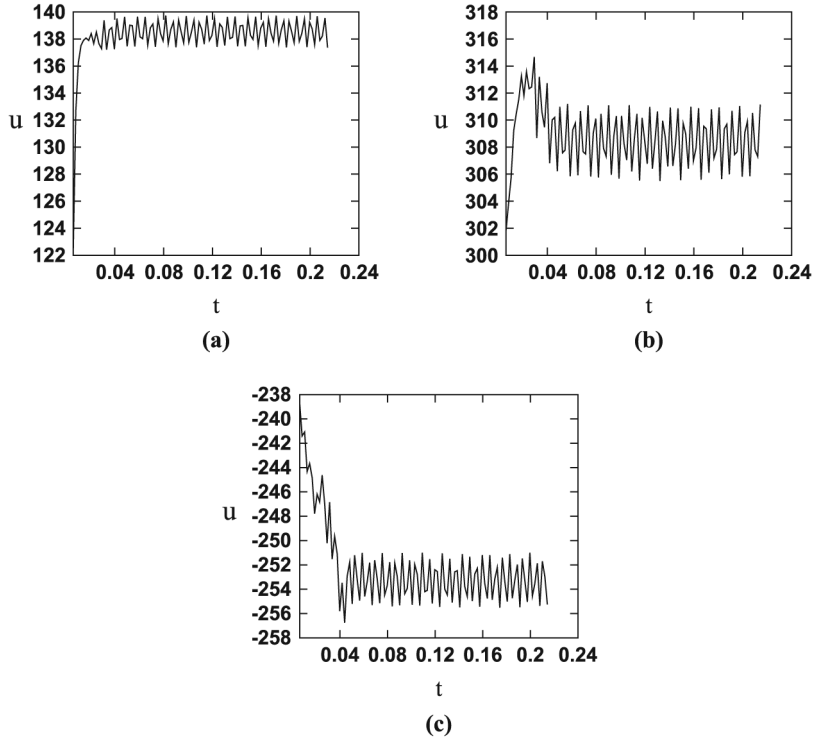

Figure 10.
Time history plots of velocity u at $\mathrm{Ra} = 4 \times 10^6$, $AR_L = 0.2$ at (a) point ①; (b) point ②; (c) point ③

a given Ra the fluid confined in the vertical leg is more prone to convection than the fluid confined in the horizontal leg.

At larger $AR_L = 0.4$, the earlier proposed idea that the penetrative convection dominates in the horizontal leg can be further strengthened if one observes the power spectrum of u at the two spatial points for $\mathrm{Ra} = 4 \times 10^6$ depicted in Figure 11. It is observed that not only the power content at point ③ is nearly ten times that at point ① but also the frequency content is higher at point ③ than at point ①. This is the result of fluctuations being generated by convecting elements in the horizontal leg supplemented by energetic fluid elements arriving from the vertical legs.

Finally, the most interesting temporal dynamics takes place for moderate AR_L and Ra, as expected because it is under these conditions that the phenomena of penetrative and non-penetrative convection in the horizontal leg compete most fiercely in an attempt to dominate. Figure 12 shows the time history of horizontal velocity u at point ③ for $\mathrm{Ra} = 2 \times 10^6$ and $AR_L = 0.3$. There is a radical alteration in the time history at a non-dimensional time of around 0.135. Since the generation of convection in the horizontal leg requires on an average lesser time (shorter distances to be covered by the buoyant

convecting elements) in comparison to the average time required by the buoyant elements generated in the vertical leg to arrive in the horizontal leg, the motion in the horizontal leg for $t \leq 0.135$ is solely due to non-penetrative convection in the horizontal leg due to its differential heating. As can be seen from the plot, the average horizontal velocity for this motion is around -150. For $t > 0.135$ the fluid from the vertical legs penetrates the horizontal leg and destroys its convection roll. This is evident from the abrupt change in the magnitude and direction of the average velocity u at point ③ from -150 to $+200$. This is a clear evidence of the phenomena of penetrative convection. It is also noticeable that this causes the velocity u to undergo a change from low frequency, large amplitude fluctuations to high frequency, small amplitude fluctuations.

Heat transfer

To study the effect of Ra and AR_L on heat transfer across the cavity the magnitude of the average Nusselt number on the hot walls BC, CD and DE (Figure 1) were computed as follows:

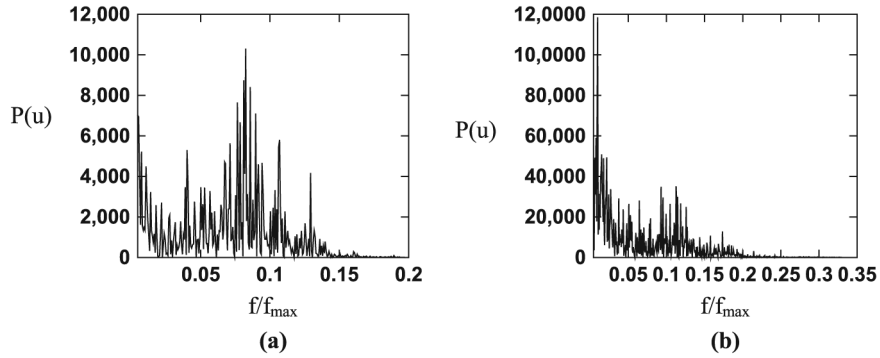

Figure 11.
Power spectrum plots of velocity u at $Ra = 4 \times 10^6$, $AR_L = 0.4$ at (a) point ①; (b) point ③

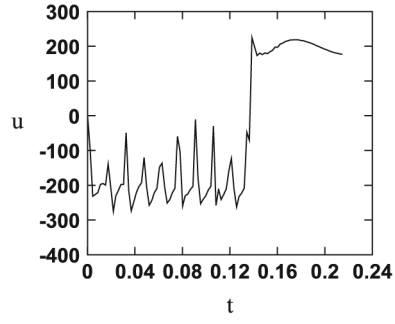

Figure 12.
Time history plot of velocity u at point ③ for $Ra = 2 \times 10^6$, $AR_L = 0.3$

$$\overline{\mathrm{Nu}}_{\mathrm{BC}} = \frac{1}{(1 - AR_{\mathrm{L}})} \int_0^{1-AR_{\mathrm{L}}} \left(\frac{\partial \theta}{\partial x} \right) \mathrm{d}y \tag{20}$$

$$\overline{\mathrm{Nu}}_{\mathrm{CD}} = \frac{1}{(1 - 2AR_{\mathrm{L}})} \int_0^{1-2AR_{\mathrm{L}}} \left(-\frac{\partial \theta}{\partial y} \right) \mathrm{d}x \tag{21}$$

$$\overline{\mathrm{Nu}}_{\mathrm{DE}} = \frac{1}{(1 - AR_{\mathrm{L}})} \int_0^{1-AR_{\mathrm{L}}} \left(-\frac{\partial \theta}{\partial x} \right) \mathrm{d}y \tag{22}$$

For unsteady flows the Nusselt numbers computed from equations (20)-(22) are functions of time as can be seen in Figure 13. The actual time variations of these average Nusselt numbers were qualitatively similar to the velocity variations with time depicted in Figures (8)-(10). From a quantitative point of view the time mean values of these average Nusselt numbers are more important. Therefore, the time mean values were calculated by integrating the time trace of the average Nusselt number over a sufficiently long interval of time and dividing by the time interval of integration. The time interval is so selected so that the initial transient is not involved in the averaging.

It was found that while average Nusselt numbers or their time mean values for wall BC and DE were identical, the average Nusselt number or its time mean value for wall CD was radically different from that of wall BC or DE. Figure 14 compares the variation of average Nusselt numbers on walls BC and CD with Ra for different AR_{L}. The range of Ra considered has been extended on the lower side to 10^3 to have a larger database for the heat transfer rates. The spatial dynamics in the vertical and the horizontal legs of the enclosure can be utilized to understand the overall heat transfer characteristics of the

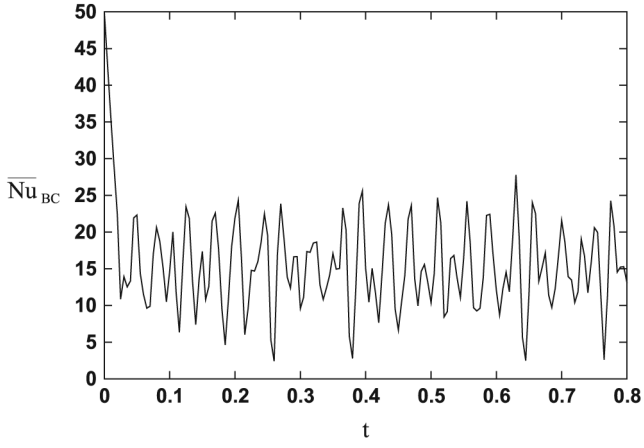

Figure 13.
Time trace of average Nusselt number on hot wall BC of the cavity at $AR_{\mathrm{L}} = 0.3$ and $\mathrm{Ra} = 4 \times 10^6$

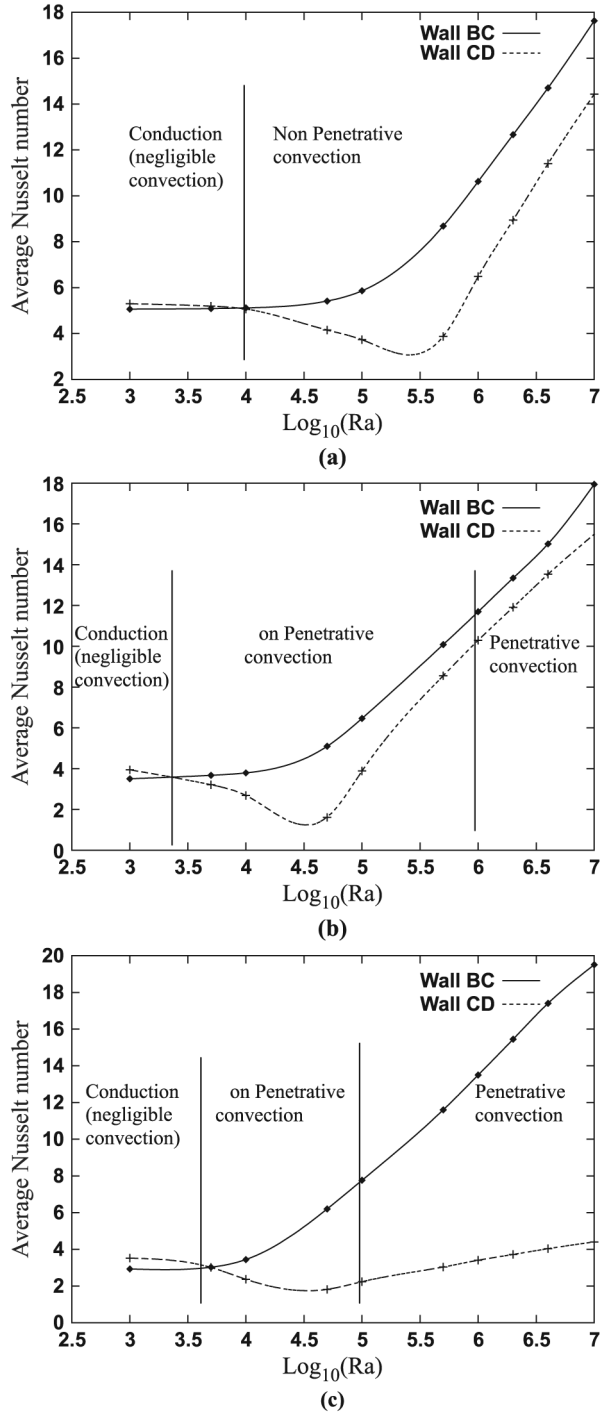

Figure 14.
Variations in average Nusselt number on hot walls of the cavity with Ra at (a) $AR_L = 0.2$; (b) $AR_L = 0.3$; (c) $AR_L = 0.4$

enclosure. As seen in Figure 14(a)-(c), while $\overline{\mathrm{Nu}}_{\mathrm{BC}}$, associated with the vertical leg, increases monotonically with Ra, the average Nusselt number for the horizontal leg $\overline{\mathrm{Nu}}_{\mathrm{CD}}$ first decreases and then begins to rise with increase in Ra. It is worth noting that for low Ra ($< 10^4$), the convective velocities are small and hence the values of $\overline{\mathrm{Nu}}_{\mathrm{BC}}$ and $\overline{\mathrm{Nu}}_{\mathrm{CD}}$ approach to those for conduction. The conduction values can be approximately found by taking a linear temperature distribution in the vertical and horizontal legs. This yields

$$\overline{\mathrm{Nu}}_{\mathrm{BC}} \cong \overline{\mathrm{Nu}}_{\mathrm{CD}} \cong \left(\frac{1}{AR_{\mathrm{L}}}\right)$$

in the conduction regime. Figure 14(a)-(c) shows good agreement with this value for low Ra ($< 10^4$). As Ra is increased, convection becomes significant and starts to control the temperature field both in the vertical and the horizontal leg of the enclosure. This is indicated in Figure 14(a)-(c) by the separation of the curves for wall BC and CD. Because the spatial flow pattern in the vertical leg comprises of formation of a single convective loop or roll, the Nusselt number for wall BC rises with increase in Ra beyond 10^4. It can also be seen from Figure 14(a)-(c) that AR_{L} has very little effect on the heat transfer characteristic of wall BC. The only significant effect of AR_{L} is to extend the regime of insignificant convection to somewhat larger Ra values for lower AR_{L}. This supports the earlier mentioned trend of suppression of convection at lower AR_{L}. It is interesting to note that in the unsteady regime ($\mathrm{Ra} > 10^6$) the time mean values of the Nusselt numbers for both walls follow the same trend as that of the steady regime.

Since the convection in the horizontal leg takes place in non-penetrative and penetrative modes, the heat transfer characteristic of wall CD exhibits some interesting features. It can readily be seen in Figure 14(a)-(c) that in the non-penetrative mode the Nusselt number for wall CD first decreases even below the near conduction values and then rises beyond a certain Ra controlled by AR_{L}. This is due to the fact that fluid in the vertical leg inevitably forms a convective loop or roll for any Ra while a threshold value of Ra or temperature gradient is needed by the fluid in the horizontal leg to form convective loops. This means that at low enough Ra, lower than the critical value needed to cause convective loops in the horizontal leg, the fluid forms convective loops in the vertical legs. The heated fluid elements in the vertical legs, rise from the walls BC and DE, and unable to penetrate into the horizontal leg owing to their low Ke, rise straight up to the cold wall where they lose heat and start to sink downwards. Since the nearly stagnant fluid in the horizontal leg gets surrounded by relatively hot rising buoyant fluid elements on both sides of the leg, the thermal diffusion from these relatively hot buoyant fluid elements reduces the thermal stratification in the horizontal leg which results in the reduction of heat transfer from wall CD. This phenomenon continues till Ra reaches a threshold value such that the fluid in the horizontal leg is able to

generate its own convection loops or rolls. As mentioned earlier in the discussion on spatial dynamics, the formation of convective loops in the horizontal leg is encouraged at larger AR_L and opposed at lower AR_L. Therefore the heat transfer rate for wall CD continues to fall upto a larger value of Ra for $AR_L = 0.2$ than for the cases of $AR_L = 0.3$ and $AR_L = 0.4$, respectively. Once the convective rolls are generated in the horizontal leg the heat transfer rate again starts to rise.

As Ra is further increased the convective loops in the horizontal leg are destroyed and the penetrative mode of convection is established. This results in further increase of heat transfer. In the penetrative mode of convection at $AR_L = 0.4$ the heat transfer from the wall CD is much less than for wall BC.

Conclusions

It has been shown that buoyancy induced motion in the odd shaped enclosure takes place in two distinct modes:

(1) non-penetrative convection, and

(2) penetrative convection. The existence of penetrative convection seems to be dependent on the Ke of the buoyant elements in the vertical legs of the enclosure which is in turn dependent on overall Ra and AR_L. The temporal dynamics exhibits the general trend of transition from steady state motion to that of periodic motion which further changes into a multi-frequency quasi-periodic motion, finally terminating into a chaotic state, with increase in Ra from 10^5 to 10^7.

For a non-penetrative convective motion, the frequency content as well as the power content in the various frequencies in a quasi-periodic state is higher in the vertical leg than in the horizontal leg. While in the case of penetrative convection it is quite opposite, with the horizontal leg exhibiting higher frequencies and more energetic fluctuations. The AR_L may be effectively utilized to control the fluctuations.

The heat transfer from the heated wall of the vertical legs is more than that from the heated wall of the horizontal leg and the penetrative mode of convection enhances the heat transfer rate from the heated wall of the horizontal leg. The AR_L has a very slight effect on the heat transfer characteristic of vertical leg while it has a significant effect on the heat transfer from the hot wall of the horizontal leg.

References

Baig, F.M. and Asrar, W. (1995), "Chaos in Rayleigh-Benard convection", *Proceeding of 2nd ISHMT-ASME International Conference on Heat and Mass transfer*, Tata-McGraw Hill Publication, New Delhi, India, pp. 211-17.

Blay, D., Tuhault, J.L. and Pinard S. (1998), "Heat transfer through a horizontal aperture connecting two non isothermal rooms", *Proceeding of 6th International Conference on Air Distributions in Rooms – ROOMVENT'98*, Stockholm, Sweden.

Coulter, J.P. and Guceri, S.I. (1987), "Laminar and turbulent natural convection within irregularly shaped enclosures", *Numerical Heat Transfer*, Vol. 12, pp. 211-27.

Curry, J.H., Herring, J.R., Loncaric, J. and Orszag, S.A. (1984), "Order and disorder in two- and three-dimensional Benard convection", *Journal of Fluid Mechanics*, Vol. 147, pp. 1-38.

Feigenbaum, M.J. (1978), "Quantitative universality for a class of nonlinear transformations", *J. Stat. Phys.*, Vol. 19, pp. 25-52.

Ferziger, J.H. and Peric, M. (1996), *Computational methods for fluid dynamics*, Springer-Verlag.

Glakpe, E.K. and Asfaw, A. (1991), "Prediction of two-dimensional natural convection in enclosures with arbitrary shapes", *Numerical Heat transfer, Part A*, Vol. 20, pp. 279-96.

Leonard, B.P. (1979), "A stable and accurate convective modelling procedure based on quadratic upstream interpolation", *Comp. Meth. Appl. Mech Eng.*, Vol. 19, pp. 59-98.

Mohamad, A.A. and Viskanta, R. (1990), "Transition to chaos in a differentially heated square cavity filled with liquid metal", in Wrobel, L.C., Brebbia, C.A. and Nowak, A.J. (Eds), *First International Conference on Advanced Computational Methods in Heat Transfer*, Springer-Verlag.

Nithiarasu, P., Seetharamu, K.N. and Sundarajan, T. (1995), "Natural convection in enclosures", *Proceedings of 2nd ISHMT-ASME International Conference on Heat and Mass transfer*, Tata-McGraw Hill Publication, New Delhi, pp. 212-17.

Nonino, C. and Croce, G. (1997), "An equal order velocity-pressure algorithm for incompressible thermal flows, part 2: validation", *Numerical Heat Transfer-Part B*, Vol. 32, pp. 17-35.

Ostrach, S. (1988), "Natural convection in enclosures", *Journal of Heat Transfer*, Vol. 110, pp. 1175-90.

Otis, D.R. and Jones, G.F. (1987), "Transient development of stratification in a partially divided enclosure", *Natural Circulation, ASME HTD*, ASME, New York, Vol. 92, pp. 307-12.

Pomeau, Y. and Manneville, P. (1980), "Intermittent transition to turbulence in dissipative systems", *Commun. Maths Phys.*, Vol. 74, pp. 189-97.

Press, W.H., Flannery, B.P., Teukolsky, S.A. and Vetterling, W.T. (1990), "Numerical recipes", Cambridge University Press.

Raji, A., Hasnaoui, M. and Zrikem, Z. (1997), "Natural convection in interacting cavities heated from below", *Int. J. Num. Meth. for Heat and Fluid Flow*, Vol. 7 No. 6, pp. 580-97.

Ruelle, D., Takens, F. and Newhouse, S.P. (1978), "Occurrence of strange attractors near quasi-periodic flows on T^m, $m > 3$", *Commun. Maths Phys.*, Vol. 64, pp. 35-40.

Yang, K.T. (1988), "Transitions and bifurcations in laminar buoyant flows in confined enclosures", *Journal of Heat Transfer*, Vol. 110, pp. 1191-204.

Yang, K.T. and Mukutmoni, D. (1993a), "Rayleigh-Benard convection in a small aspect ratio enclosure: part I-bifurcation to oscillatory convection", *Journal of Heat Transfer*, Vol. 115, pp. 360-6.

Yang, K.T. and Mukutmoni, D. (1993b), "Rayleigh-Benard convection in a small aspect ratio enclosure: part II-bifurcation to chaos", *Journal of Heat Transfer*, Vol. 115, pp. 367-76.